21. M. K. Pető, S. Mukhopadhyay, K. A. Kelley, *Earth Planet. Sci. Lett.* **369–370**, 13–23 (2013).
22. M. G. Jackson, S. B. Shirey, E. H. Hauri, M. D. Kurz, H. Rizo, *Geochim. Cosmochim. Acta* 10.1016/j.gca.2016.02.011 (2016).
23. J. P. Brandenburg, E. H. Hauri, P. E. van Keken, C. J. Ballentine, *Earth Planet. Sci. Lett.* **276**, 1–13 (2008).
24. E. J. Garnero, A. K. McNamara, *Science* **320**, 626–628 (2008).
25. M. Horan, R. J. Walker, J. W. Morgan, J. N. Grossman, A. E. Rubin, *Chem. Geol.* **196**, 27–42 (2003).
26. T. J. Ireland, R. J. Walker, M. O. Garcia, *Chem. Geol.* **260**, 112–128 (2009).
27. W. B. Tonks, H. J. Melosh, *J. Geophys. Res. Planets* **98**, 5319–5333 (1993).

ACKNOWLEDGMENTS

We thank T. Mock for assistance with mass spectrometry. This work was improved by helpful discussions with J. O'Neil, S. Shirey, and B. Wood. We thank S. Shirey, who provided sample VE-32. We also appreciate the helpful comments and suggestions from three anonymous reviewers. We thank M. Garçon, who developed the four-step ^{142}Nd acquisition method. This work was supported by NSF grant EAR-1265169 (Cooperative Studies of the Earth's Deep Interior program) to R.J.W. and grant EAR-1250419 to S.M. All data are available in the main manuscript and supplementary materials.

SUPPLEMENTARY MATERIALS

www.sciencemag.org/content/352/6287/809/suppl/DC1
Materials and Methods
Figs. S1 to S6
Tables S1 to S5
References (*28*–*56*)

12 November 2015; accepted 5 April 2016
10.1126/science.aad8563

SLEEP RESEARCH

Causal evidence for the role of REM sleep theta rhythm in contextual memory consolidation

Richard Boyce,[1] Stephen D. Glasgow,[2] Sylvain Williams,[2]*† Antoine Adamantidis[2,3]*†

Rapid eye movement sleep (REMS) has been linked with spatial and emotional memory consolidation. However, establishing direct causality between neural activity during REMS and memory consolidation has proven difficult because of the transient nature of REMS and significant caveats associated with REMS deprivation techniques. In mice, we optogenetically silenced medial septum γ-aminobutyric acid–releasing (MS^{GABA}) neurons, allowing for temporally precise attenuation of the memory-associated theta rhythm during REMS without disturbing sleeping behavior. REMS-specific optogenetic silencing of MS^{GABA} neurons selectively during a REMS critical window after learning erased subsequent novel object place recognition and impaired fear-conditioned contextual memory. Silencing MS^{GABA} neurons for similar durations outside REMS episodes had no effect on memory. These results demonstrate that MS^{GABA} neuronal activity specifically during REMS is required for normal memory consolidation.

The physiological function of rapid eye movement sleep (REMS) is unclear (*1*). Evidence linking REMS to aspects of memory consolidation in mammals has been obtained using techniques such as statistical correlation, pharmacology, and REMS deprivation (*2*, *3*). However, whether REMS has a direct role in learning and memory remains controversial; correlative studies are not definitive, REMS has a transient pattern of occurrence that prevents REMS-selective pharmacological manipulation, and REMS deprivation has critical caveats that are difficult to fully control for (*4*, *5*).

During REMS in mice and rats, a prominent ~7-Hz theta oscillation is observed in local field potential (LFP) recordings from cortical structures, including the hippocampus (*6*, *7*). Hippocampal theta rhythms during REMS may contribute to memory consolidation by providing a mechanism for strengthening place cells formed during prior wakefulness (*8*, *9*). Theta rhythm generation requires an intact medial septum (MS) (*10*, *11*), although the MS is not involved in REMS generation itself (*12*, *13*). MS γ-aminobutyric acid–releasing (MS^{GABA}) neurons project to the hippocampus, probably pacing the hippocampal theta rhythm during REMS (*14*–*16*). In mice, we therefore used optogenetics to silence MS^{GABA} neurons and reduce theta activity selectively during REMS, without disturbing sleeping behavior, to determine whether intact MS^{GABA} neural activity during REMS is important for memory consolidation.

Adeno-associated virus (AAVdj) encoding Archaerhodopsin fused to an enhanced yellow fluorescent protein (eYFP) reporter (ArchT-eYFP) was injected into the MS of VGAT::Cre mice (Fig. 1A, top). The resulting ArchT-eYFP expression was ~95% specific for MS^{GABA} neurons (Fig. 1A, bottom, and fig. S1A), stable, and localized to the MS and the diagonal band of Broca (DBB) region for at least 3 months after injection. MS^{GABA} neural projections were observed throughout the hippocampus (Fig. 1B).

Whole-cell voltage and current clamp recordings of ArchT-eYFP–expressing MS neurons in acute brain slices (fig. S1B) revealed hyperpolarization (−39.9 ± 6.6 mV) and outward current (293.9 ± 69.2 pA) upon 594-nm light exposure (fig. S1B). Single-unit recordings in behaving transfected mice (fig. S1C) confirmed that photoinhibition during REMS, non-REM sleep (NREMS), and wakefulness rapidly produced a potent and reversible reduction in spiking of putative MS^{GABA} neurons (fig. S1D).

We next tested the effect of silencing MS^{GABA} neurons during REMS in freely behaving mice. Photoinhibition with constant light pulses delivered to the MS in ArchT-eYFP–expressing mice (ArchT mice) resulted in significantly (65.3 ± 5.6%) reduced theta power measured from dorsal hippocampal area CA1 LFP (CA1LFP) recording (Fig. 1D, top). No other frequency bands were affected, and the spectral profile of the CA1LFP returned to baseline levels almost immediately upon release of MS^{GABA} neurons from photoinhibition (Fig. 1D, top, and Fig. 2A). Current source density (CSD) analysis revealed that reduced theta power was present in all layers of dorsal hippocampal CA1 (Fig. 2B). Light pulses delivered to the MS of mice only expressing eYFP in MS^{GABA} neurons (YFP control mice) did not affect CA1LFP power (Fig. 1D, bottom), ruling out light as a potential confounding factor in these results. Inhibition of MS^{GABA} neurons did not perturb sleeping behavior (Fig. 1D, top), and the probability of state transition during REMS in ArchT mice was unaltered relative to YFP control mice (n = 30 ArchT mice, n = 19 YFP control mice; P = 0.63, unpaired Student's t test).

We optogenetically silenced MS^{GABA} neurons selectively during each REMS episode after acquisition of a novel object place recognition (NOPR) task (Fig. 3A). Mice showed no preference for either object during initial object habituation [day 1 (D1), task acquisition] (Fig. 3A, right). After acquisition, EEG/CA1LFP/EMG (EEG, electroencephalogram; EMG, electromyogram) activity was monitored for 4 hours. Upon entry into REMS, mice in the ArchT or YFP control group had light continuously delivered to the MS until transition to another state occurred, at which time light delivery ceased until subsequent REMS was detected (Fig. 3B). A group of ArchT-eYFP expressing mice that never received light (ArchT control) served as a baseline control for ArchT-eYFP transfection. To determine whether REMS was a critical factor in our results, a final group

[1]Integrated Program in Neuroscience, McGill University, Montreal, Quebec, Canada. [2]Department of Psychiatry, McGill University, Montreal, Quebec, Canada. [3]Department of Neurology and Department of Clinical Research, Inselspital University Hospital, University of Bern, Bern, Switzerland.
*Corresponding author. Email: sylvain.williams@douglas.mcgill.ca (S.W.); antoine.adamantidis@dkf.unibe.ch (A.A.) †These authors contributed equally to this work.

of mice expressing ArchT-eYFP (ArchT REM control) underwent the same protocol as mice in the ArchT group, with the exception that light delivery to the MS was delayed upon detection of REMS by ~5 min (supplementary methods). After the delay, light was delivered continuously to the MS for a duration equaling that of the preceding REMS episode. The result was a pattern of inhibition that, whereas statistically similar to the REMS-specific pattern that ArchT mice received, occurred primarily when mice were not engaged in REMS. MS^{GABA} neurons were inhibited during 91.6 ± 1.3% of the cumulative REMS duration occurring during the post-test period in ArchT mice (Fig. 3C, top, and fig. S3A), with little inhibition during other states (Fig. 3C, top; laser on 0.2 ± 0.0% of NREMS; 1.5 ± 0.2% of wakefulness). Sleep architecture was unaffected by REMS-selective MS^{GABA} neural photoinhibition during the 4-hour post-test period (fig. S3, A and B), and the only significant effect on the CA1LFP spectral profile (Fig. 3C, bottom, and figs. S4, A to C, and S5C) was reduced (60.2 ± 2.4%) REMS theta power. Basic firing activity during wakefulness, NREMS, and REMS of isolated single neurons recorded at the dorsal CA1 cell layer in a subset of mice during the 4-hour post-test period (supplementary methods) was unaffected by REMS-specific MS^{GABA} neural inhibition (fig. S6, A and B). Analysis of REMS immediately after the 4-hour post-test period when optogenetic silencing of MS^{GABA} neurons during REMS had ceased (4- to 5-hour post-test/recovery period) revealed an immediate return of REMS CA1LFP spectral power to baseline levels (fig. S4, B and C) and no alteration in cumulative and average episode durations in ArchT mice relative to controls (fig. S3C). EEG spindles (tables S1 to S3) and hippocampal ripples (tables S6 to S9) measured during NREMS throughout the course of the NOPR protocol were also unaltered.

On day 2 (D2), object 2 was moved to a new location while object 1 remained stationary (Fig. 3D, left). Because mice preferentially investigate novel stimuli, if object orientation memory is intact, mice should intrinsically investigate object 2 more than object 1 (*17*). Preference for object 2 [object 2 discrimination index (DI), supplementary methods] was not different relative to D1 testing in ArchT mice (Fig. 3D, right, and 3E). This result is not due to the MS light delivery method, because YFP control mice that underwent the same light delivery protocol (Fig. 3C, top; laser on 86.8 ± 4.6% of REMS; 0.2 ± 0.1% of NREMS; 2.7 ± 0.3% of wakefulness) had higher D2 object 2 DI relative to neutral D1 discrimination (Fig. 3D, right, and 3E). ArchT control mice also had increased object 2 DI during D2 testing from neutrality observed on D1 (Fig. 3D, right, and 3E). The co-occurrence of MS^{GABA} neural inhibition with REMS was a critical factor in the deficit observed in ArchT mice, because ArchT REM control mice demonstrated intact object recognition memory comparable to that of YFP control and ArchT control mice (Fig. 3D, right, and 3E). No evidence for differences in locomotion or motivation during testing were found between groups (fig. S5, A and B).

We next investigated whether normal contextual and emotional memory consolidation requires MS^{GABA} neural activity (Fig. 4). ArchT, YFP control, ArchT control, and ArchT REM control mice were fear-conditioned in a distinct context (context A) with three tone-shock events spanning a 9.5-min session. Freezing behavior between groups was not different during conditioning (Fig. 4A). For the subsequent 4 hours, a protocol similar to that used after D1 NOPR testing was again used

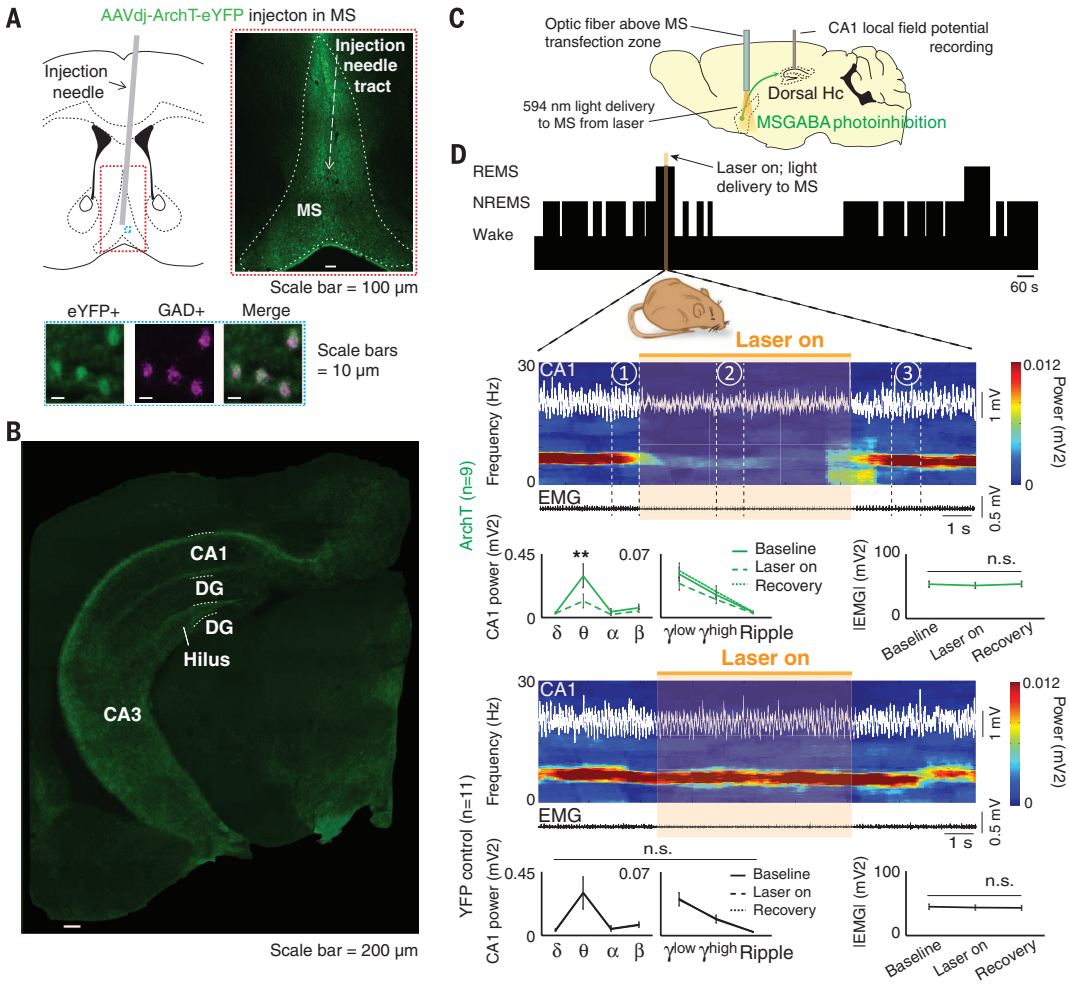

Fig. 1. ArchT-mediated inhibition of MS^{GABA} neurons during REMS reduces theta rhythm. (**A**) Schematic (top left) showing the MS injection site of Cre-dependent AAV in VGAT::Cre mice. After virus delivery, ArchT-eYFP is inverted in MS^{GABA} neurons, allowing transcription from the EF-1α promoter and subsequent expression of ArchT-eYFP to occur in the MS (top right). (Bottom) Cell-specific expression of ArchT-eYFP (green) in MS^{GABA} [glutamic acid decarboxylase (GAD^{+})] neurons (magenta) (quantified in fig. S1A). (**B**) Dense projections in the hippocampus originating from MS^{GABA} neurons (green). DG, dentate gyrus. (**C**) Schematic of the in vivo recording configuration; an optic fiber delivered orange laser light to the MS, allowing for optogenetic inhibition of MS^{GABA} neurons while recording the LFP signal from electrodes implanted in dorsal CA1. (**D**) Effect of MS^{GABA} neural inhibition during REMS on CA1LFP and EMG activity. Mice injected with a control virus resulting in expression of only eYFP in MS^{GABA} neurons controlled for the use of orange light (YFP control) [n = 9 for ArchT mice, n = 11 for YFP control mice; n.s. = not significant, $^{**}P < 0.01$, two-way analysis of variance (ANOVA) with Tukey post-hoc test].

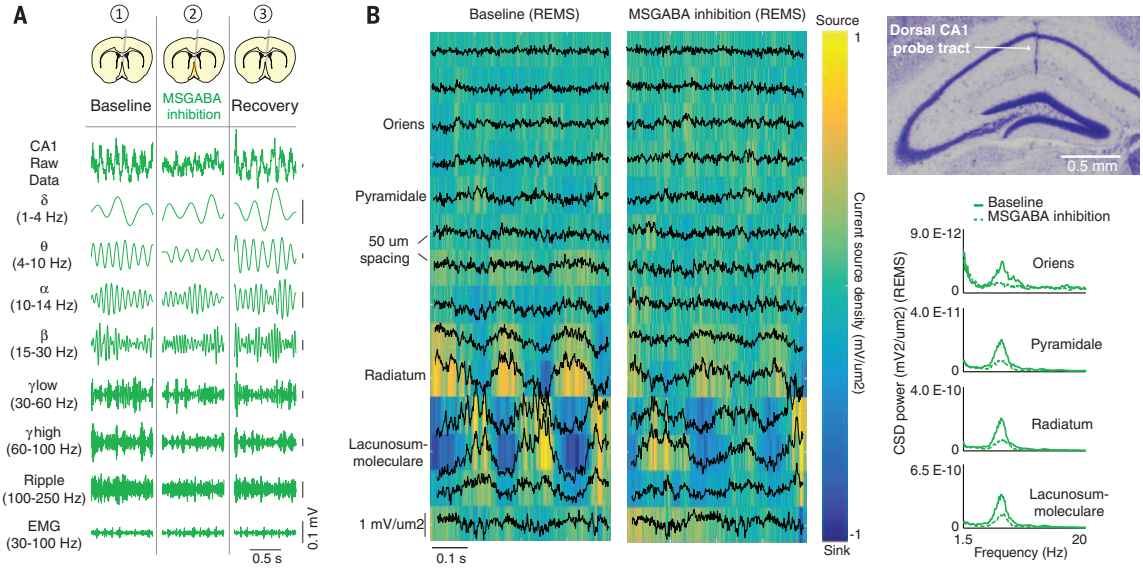

Fig. 2. MS^{GABA} neural silencing during REMS reduces theta power in all layers of dorsal hippocampal CA1. (**A**) Sample raw and filtered traces from ArchT example trace in Fig. 1D, as indicated. Recordings were from the stratum radiatum of dorsal hippocampal CA1. (**B**) (Left) CSD analysis completed on recordings obtained from dorsal hippocampal CA1 (top right) using a chronically implanted linear 16-channel probe (50 μm spacing between successive channels) during REMS under baseline and MS^{GABA} neural inhibition conditions. Graphs at right show layer-specific spectral analysis of CSDs for the baseline versus the MS^{GABA} neural inhibition condition (n = 1 AAVdj-ArchT–injected mouse).

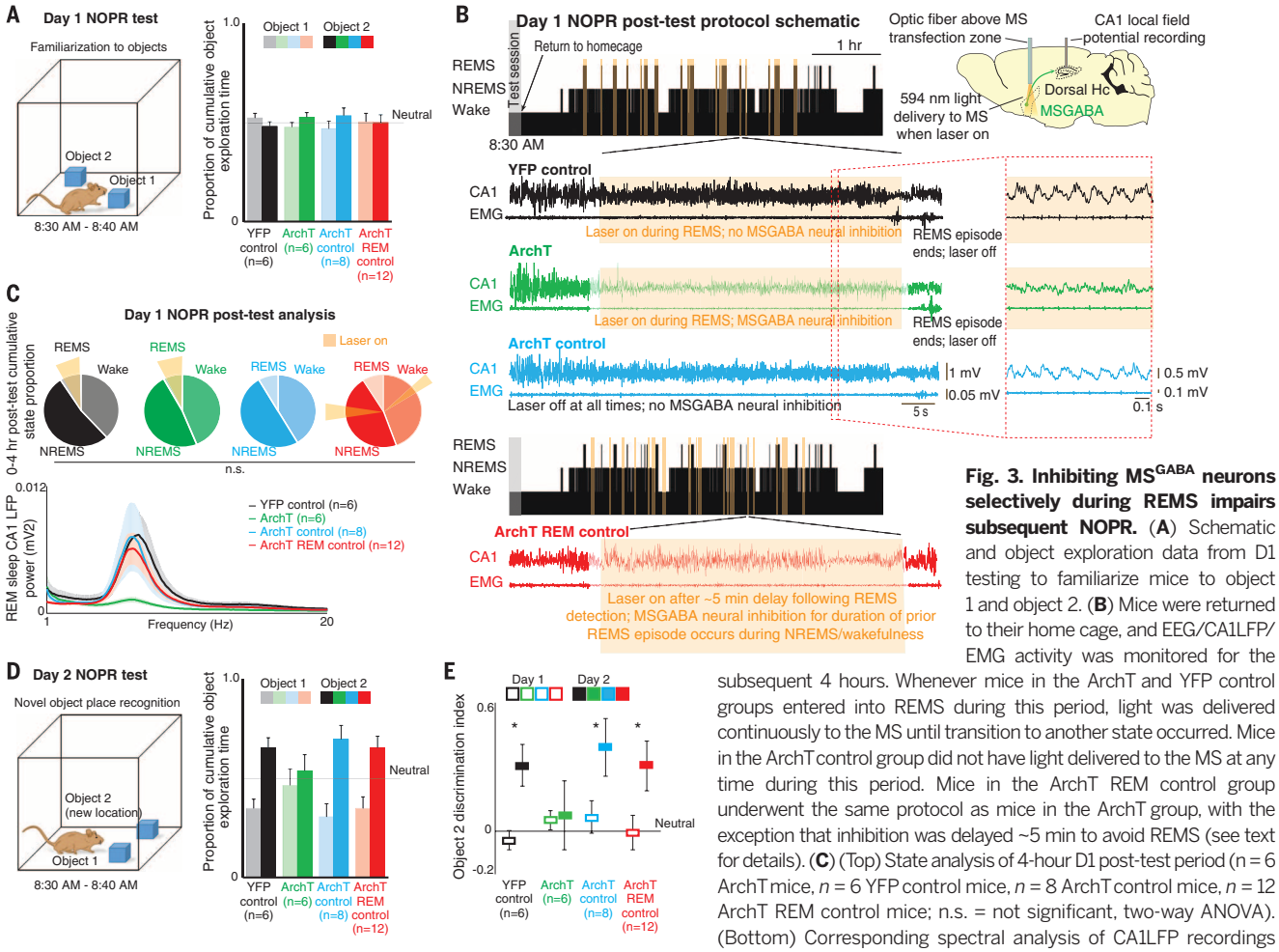

Fig. 3. Inhibiting MS^{GABA} neurons selectively during REMS impairs subsequent NOPR. (**A**) Schematic and object exploration data from D1 testing to familiarize mice to object 1 and object 2. (**B**) Mice were returned to their home cage, and EEG/CA1LFP/EMG activity was monitored for the subsequent 4 hours. Whenever mice in the ArchT and YFP control groups entered into REMS during this period, light was delivered continuously to the MS until transition to another state occurred. Mice in the ArchT control group did not have light delivered to the MS at any time during this period. Mice in the ArchT REM control group underwent the same protocol as mice in the ArchT group, with the exception that inhibition was delayed ~5 min to avoid REMS (see text for details). (**C**) (Top) State analysis of 4-hour D1 post-test period (n = 6 ArchT mice, n = 6 YFP control mice, n = 8 ArchT control mice, n = 12 ArchT REM control mice; n.s. = not significant, two-way ANOVA). (Bottom) Corresponding spectral analysis of CA1LFP recordings during REMS. (**D**) Schematic and object exploration data from D2 testing; only object 2 placement differed relative to D1. (**E**) Analysis of object 2 preference between D1 and D2 (n = 6 ArchT mice, n = 6 YFP control mice, n = 8 ArchT control mice, n = 12 ArchT REM control mice; *P < 0.05, paired Student's t test).

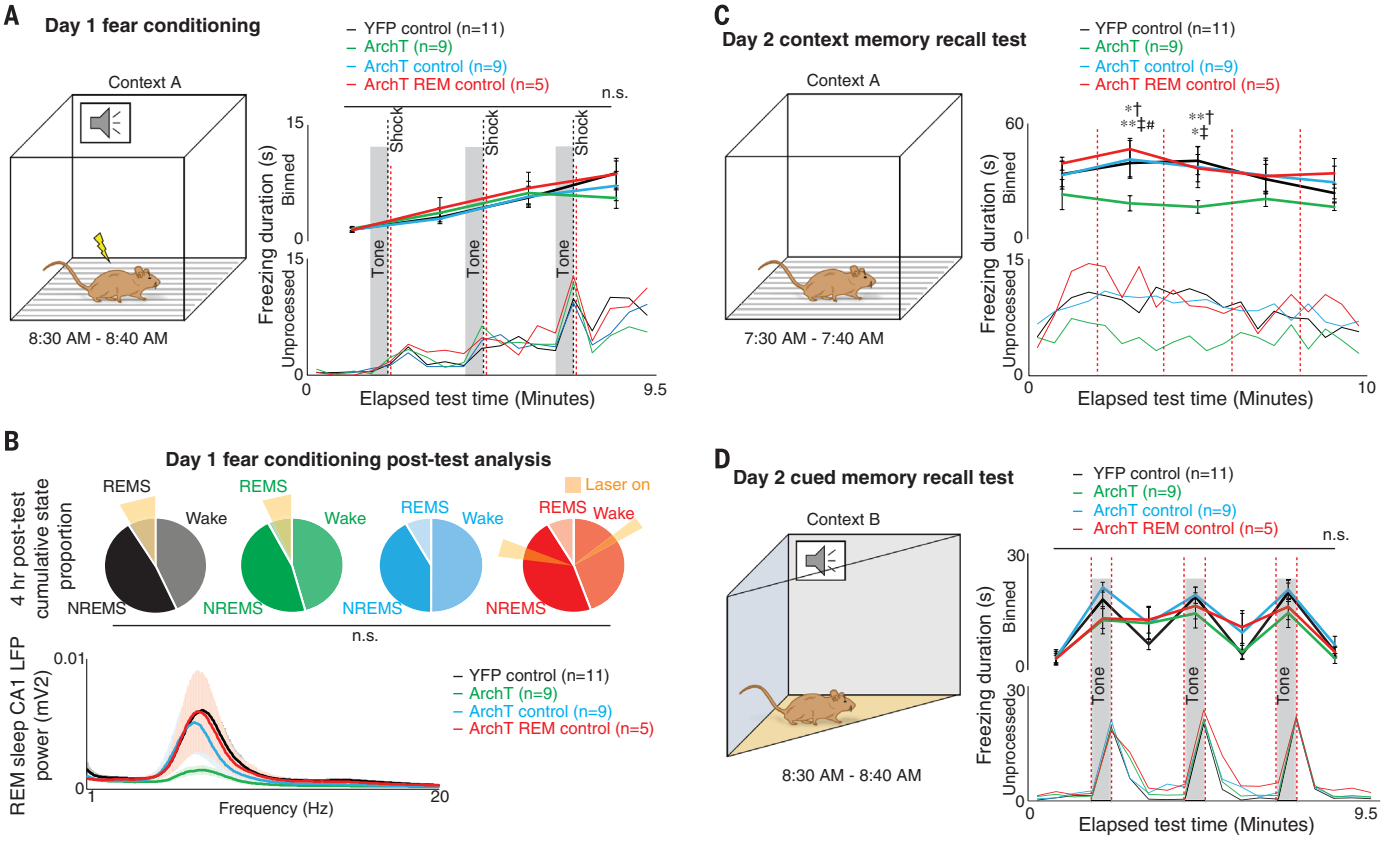

Fig. 4. Inhibiting MS^{GABA} neurons selectively during REMS after fear conditioning impairs contextual memory. (**A**) Fear conditioning schematic and freezing data. (**B**) Immediately after conditioning, mice were returned to their home cage, where they underwent the same procedure as that described after D1 NOPR testing (a full schematic is in Fig. 3B). (Top) State analysis of 4-hour post-conditioning period (n = 9 ArchT mice, n = 11 YFP control mice, n = 9 ArchT control mice, n = 5 ArchT REM control mice; n.s. = not significant, two-way ANOVA). (Bottom) Corresponding spectral analysis of CA1LFP recordings during REMS. (**C**) D2 contextual recall memory test schematic and freezing analysis. (**D**) D2 cued recall memory test schematic and freezing analysis. (A), (C), and (D) Freezing versus time graphs (n = 9 ArchT mice, n = 11 YFP control mice, n = 9 ArchT control mice, n = 5 ArchT REM control mice; n.s. = not significant, *P < 0.05, **P < 0.01, two-way repeated-measures ANOVA with Tukey post-hoc test; †YFP control versus ArchT mice, ‡ArchT control versus ArchT mice, #ArchT REM control versus ArchT mice). (A) and (D) Statistical results confirmed with Kruskal-Wallis test. Red lines indicate unprocessed data bin boundaries used for statistics (top right plot).

(see Fig. 3B for a detailed schematic). ArchT mice received selective MS^{GABA} neural inhibition during REMS (laser on 92.2 ± 2.2% of REMS; 0.2 ± 0.0% of NREMS; 1.6 ± 0.2% of wakefulness) during the 4-hour post–fear conditioning period (Fig. 4B). No difference in sleep-wake architecture (Fig. 4B, top, and fig. S7, A to C) or NREMS EEG spindle activity (tables S4 and S5) was found between groups, and the only significant effect on the CA1LFP spectral profile was a 57.8 ± 5.7% reduction in theta power in ArchT mice (Fig. 4B, bottom, and fig. S8, A to C).

The next day mice were first tested for contextual recall memory (Fig. 4C) followed by cued recall memory (Fig. 4D). Mice were placed in context A for 10 min, where conditioning had occurred the prior day, and allowed to move freely without any tone or shock. ArchT mice froze less than YFP control, ArchT control, and ArchT REM control mice (Fig. 4C, right). One hour later, mice were placed in a novel context (context B) for 9.5 min for cued recall testing, and a sequence of tones identical to those from prior fear conditioning was played. Freezing behavior was not different between the ArchT, YFP control, ArchT control, or ArchT REM control groups, with each group showing a robust freezing response selectively to the cue (tone) (Fig. 4D, right).

NOPR and fear-conditioned contextual memory in these experiments were probably hippocampus-dependent (*18*, *19*). Considering the potential importance of hippocampal REMS theta oscillations in processing place cell information (*8*, *9*), the impairments reported here could result from disrupted theta-dependent plasticity in hippocampal neurons during REMS after initial memory consolidation. REMS may also contribute to the homeostasis of network excitability (*20*, *21*). Disruption of hippocampal homeostasis could have contributed to the memory impairment we observed, although analysis of CA1 unit data did not reveal any clear indication of altered activity resulting from MS^{GABA} neural inhibition during REMS. Extrahippocampal inputs also must be considered, given known MS projection patterns (*22*). Indeed, current source density analysis from CA1 during REMS indicated a reduction in theta rhythm power at all layers upon MS^{GABA} neural inhibition. Thus, in addition to disrupted input from the Schaffer-collaterals, input from the entorhinal cortex via the perforant path was also disrupted. Given the importance of these inputs in spatial memory and hippocampal place cell activity (*18*, *23*), their disruption may be a mechanism involved in the blockade of consolidation we observed. In summary, our data provide experimental proof in a mouse model that MS^{GABA} neural activity occurring specifically during REMS after acquisition of a NOPR task or fear conditioning is critical for normal spatial and contextual memory consolidation.

REFERENCES AND NOTES

1. J. M. Siegel, *Nature* **437**, 1264–1271 (2005).
2. S. Diekelmann, J. Born, *Sleep* **11**, 114–126 (2010).
3. R. Stickgold, M. P. Walker, *Sleep* **28**, 1225–1227 (2005).
4. J. M. Siegel, *Science* **294**, 1058–1063 (2001).

5. R. P. Vertes, *Neuron* **44**, 135–148 (2004).
6. T. E. Robinson, R. C. Kramis, C. H. Vanderwolf, *Brain Res.* **124**, 544–549 (1977).
7. G. Buzsáki, *Neuron* **33**, 325–340 (2002).
8. G. R. Poe, D. A. Nitz, B. L. McNaughton, C. A. Barnes, *Brain Res.* **855**, 176–180 (2000).
9. K. Louie, M. A. Wilson, *Neuron* **29**, 145–156 (2001).
10. J. D. Green, A. A. Arduini, *J. Neurophysiol.* **17**, 533–557 (1954).
11. S. J. Mitchell, J. N. Rawlins, O. Steward, D. S. Olton, *J. Neurosci.* **2**, 292–302 (1982).
12. B. E. Jones, *Neuroscience* **40**, 637–656 (1991).
13. R. E. Brown, R. Basheer, J. T. McKenna, R. E. Strecker, R. W. McCarley, *Physiol. Rev.* **92**, 1087–1187 (2012).
14. H. Petsche, C. Stumpf, G. Gogolak, *Electroencephalogr. Clin. Neurophysiol.* **14**, 202–211 (1962).
15. A. P. Simon, F. Poindessous-Jazat, P. Dutar, J. Epelbaum, M. H. Bassant, *J. Neurosci.* **26**, 9038–9046 (2006).
16. K. Tóth, T. F. Freund, R. Miles, *J. Physiol.* **500**, 463–474 (1997).
17. M. Antunes, G. Biala, *Cogn. Process.* **13**, 93–110 (2012).
18. M. B. Moser, D. C. Rowland, E. I. Moser, *Cold Spring Harbor Perspect. Biol.* **7**, 1–15 (2016).
19. J. J. Kim, M. S. Fanselow, *Science* **256**, 675–677 (1992).
20. A. A. Borbély, *Hum. Neurobiol.* **1**, 195–204 (1982).
21. A. D. Grosmark, K. Mizuseki, E. Pastalkova, K. Diba, G. Buzsáki, *Neuron* **75**, 1001–1007 (2012).
22. R. C. Meibach, A. Siegel, *Brain Res.* **119**, 1–20 (1977).
23. M. E. Hasselmo, *Eur. J. Neurosci.* **28**, 1301–1315 (2008).

ACKNOWLEDGMENTS

We thank all members of the Williams and Tidis labs for their helpful comments on the manuscript, E. Boyden for viral constructs, and B. Lowell and L. Vong for mice. R.B. was supported by an Alexander Graham Bell Canada Graduate Scholarship [Natural Sciences and Engineering Research Council of Canada (NSERC)] while completing this research. S.D.G. was supported by a postdoctoral fellowship from Fonds de la Recherche en Santé du Québec. S.W. is supported by the Canadian Institutes of Health Research (CIHR) and NSERC. A.A. is supported by the Human Frontier Science Program (RGY0076/2012), the Douglas Foundation, McGill University, the Canadian Fund for Innovation (CFI), the Canadian Research Chair (CRC Tier 2), CIHR, NSERC, the Swiss National Science Foundation, the Inselspital, and the University of Bern. All data are available in the supplementary materials. We declare no conflicts of interest.

SUPPLEMENTARY MATERIALS

www.sciencemag.org/content/352/6287/812/suppl/DC1
Materials and Methods
Figs. S1 to S8
Tables S1 to S9
References (*24*–*27*)

9 October 2015; accepted 24 March 2016
10.1126/science.aad5252

ZIKA VIRUS

Zika virus impairs growth in human neurospheres and brain organoids

Patricia P. Garcez,[2,1]* Erick Correia Loiola,[1]† Rodrigo Madeiro da Costa,[1]† Luiza M. Higa,[3]† Pablo Trindade,[1]† Rodrigo Delvecchio,[3] Juliana Minardi Nascimento,[1,4] Rodrigo Brindeiro,[3] Amilcar Tanuri,[3] Stevens K. Rehen[1,2]*

Since the emergence of Zika virus (ZIKV), reports of microcephaly have increased considerably in Brazil; however, causality between the viral epidemic and malformations in fetal brains needs further confirmation. We examined the effects of ZIKV infection in human neural stem cells growing as neurospheres and brain organoids. Using immunocytochemistry and electron microscopy, we showed that ZIKV targets human brain cells, reducing their viability and growth as neurospheres and brain organoids. These results suggest that ZIKV abrogates neurogenesis during human brain development.

Primary microcephaly is a severe brain malformation characterized by the reduction of the head circumference. Patients display a heterogeneous range of brain impairments that compromise motor, visual, hearing, and cognitive functions (*1*).

Microcephaly is associated with decreased neuronal production as a consequence of proliferative defects and death of cortical progenitor cells (*2*). During pregnancy, the primary etiology of microcephaly varies from genetic mutations to external insults. The so-called TORCHS factors (toxoplasmosis, rubella, cytomegalovirus, herpes virus, and syphilis) are the main congenital infections that compromise brain development in utero (*3*).

[1]D'Or Institute for Research and Education (IDOR), Rio de Janeiro, Brazil. [2]Institute of Biomedical Sciences, Federal University of Rio de Janeiro, Rio de Janeiro, Brazil. [3]Institute of Biology, Federal University of Rio de Janeiro, Rio de Janeiro, Brazil. [4]Institute of Biology, State University of Campinas, Campinas, Brazil.
***Corresponding author. Email: ppgarcez@icb.ufrj.br (P.P.G.); srehen@lance-ufrj.org (S.K.R.)** †These authors contributed equally to this work.

An increase in the rate of microcephaly in Brazil has been associated with the recent outbreak of Zika virus (ZIKV) (*4*, *5*), a flavivirus that is transmitted by mosquitoes (*6*) and sexually (*7*–*9*). So far, ZIKV has been described in the placenta and amniotic fluid of microcephalic fetuses (*10*–*13*) and in the blood of microcephalic newborns (*11*, *14*). ZIKV had also been detected within the brain of a microcephalic fetus (*13*, *14*), and recently, direct evidence has emerged that ZIKV is able to infect and cause the death of neural stem cells (*15*).

We used human induced pluripotent stem (iPS) cells cultured as neural stem cells (NSCs), neurospheres, and brain organoids to explore the consequences of ZIKV infection during neurogenesis and growth with three-dimensional culture models. Human iPS-derived NSCs were exposed to ZIKV [multiplicity of infection (MOI), 0.25 to 0.0025]. After 24 hours, ZIKV was detected in NSCs (Fig. 1, A to D); viral envelope protein was evident in 10.10% (MOI, 0.025) and 21.7% (MOI, 0.25) of cells exposed to ZIKV (Fig. 1E). Viral RNA was also detected in the supernatant of infected NSCs (MOI, 0.0025) by quantitative reverse transcriptase polymerase chain reaction (qRT-PCR) (Fig. 1F), providing evidence of productive infection.

To investigate the effects of ZIKV during neural differentiation, mock- and ZIKV-infected NSCs were cultured as neurospheres. After 3 days in vitro (DIV), mock-infected NSCs generated round neurospheres. However, ZIKV-infected NSCs generated neurospheres with morphological abnormalities and cell detachment (Fig. 2B). After 6 DIV, hundreds of neurospheres grew under mock conditions (Fig. 2, C and E). In ZIKV-infected NSCs (MOI, 2.5 to 0.025), only a few neurospheres survived (Fig. 2, D and E).

Mock-infected neurospheres presented the expected ultrastructural morphology of the nucleus and mitochondria (Fig. 3A). Viral particles were present in ZIKV-infected neurospheres, similar to those observed in murine glial and neuronal cells (*16*). ZIKV was bound to the membranes and observed in mitochondria and vesicles of cells within infected neurospheres (arrows in Fig. 3, B and F). Apoptotic nuclei, a hallmark of cell death, were observed in all ZIKV-infected neurospheres that we analyzed (Fig. 3B). ZIKV-infected cells in neurospheres presented smooth membrane structures (Fig. 3, B and F), similar to other cell types infected with dengue virus (*17*). These results suggest that ZIKV induces cell death in human neural stem cells and thus impairs the formation of neurospheres.

To further investigate the impact of ZIKV infection during neurogenesis, human iPS-derived brain organoids (*18*) were exposed to ZIKV and observed for 11 DIV (Fig. 4). The growth rates of 12 individual organoids (six mock- and six ZIKV-infected) were measured during this period (Fig. 4, A to D). As a result of ZIKV infection, the average growth area of ZIKV-exposed organoids was reduced by 40% compared with brain organoids under mock conditions [0.624 ± 0.064 mm^2 for ZIKV-exposed organoids versus 1.051 ± 0.1084 mm^2 for mock-infected organoids (normalized); Fig. 4E].

Causal evidence for the role of REM sleep theta rhythm in contextual memory consolidation

Richard Boyce, Stephen D. Glasgow, Sylvain Williams and Antoine Adamantidis

Science **352** (6287), 812-816.
DOI: 10.1126/science.aad5252

Let sleeping mice remember

The role of REM (rapid eye movement) sleep for memory consolidation has been discussed for a long time. Boyce *et al.* used optogenetics to inhibit theta oscillations in the mouse hippocampus during REM sleep (see the Perspective by Kocsis). Both object recognition memory and contextual fear memory were impaired. This consolidation mechanism occurred in a critical time window immediately after training. Disrupting the same system for similar durations during non-REM sleep or wakefulness had no effect on memory.

Science, this issue p. 812; see also p. 770